New Methods for the Calculation of the Load Capacity of Bevel and Hypoid Gears

Christian Wirth, Bernd-Robert Höhn and Christo Braykoff

Flank breakage is common in a number of cylindrical and bevel gear applications. This paper introduces a relevant, physically based calculation method to evaluate flank breakage risk vs. pitting risk. Verification of this new method through testing is demonstrably shown.

Introduction

Flank breakage in cylindrical and bevel gear applications typically initiates in the active flank, approximately in the middle of the active tooth height, and subsequently propagating to the tooth root of the unloaded flank side.

Crack initiation can be localized below the surface in the region between the case and core of surface-hardened gears. This failure mode cannot be explained by known causes such as tooth root breakage or pitting. Even bevel gears in truck and bus applications are at risk of damage from sub-surface fatigue if an optimum utilization of material is not achieved. In such cases a balance between the flank breakage and pitting risk must be struck. This paper describes a new "material-physical-based calculation" method to evaluate risk of flank breakage vs. pitting damage. This method was used to improve the design of a gear set that failed in several cases due to flank breakage on the wheel in test vehicles of MAN Truck & Bus (MTB). Figure 1 shows a typically damaged tooth on the wheel. In some cases pitting occurred on the coast flanks of the wheel (Fig. 1 — right). The following demonstrates how it is possible to increase the load capacity of the wheel regarding pitting and flank breakage by means of this new method, as proven in successful test runs.

Flank Breakage in Bevel Gears

Flank breakage often appears without any of the other commonly seen surface failures such as scuffing, pitting or micro-pitting. In some cases only one tooth is affected, but usually more than one tooth fails (Fig. 2). Inadequate material properties and heat treatment are expected to increase the risk of flank breakage, especially insufficient core strength and toughness, or insufficient—or too high—case depths (Refs. 4–5). In many U.S. publications flank breakage is also called "sub-surface fatigue" or "sub-case fatigue." In

these papers the flank pressure is also regarded as the decisive parameter (Refs. 2, 6, 13, 15, 16).

By virtue of systematic tests, Annast (Ref. 1) investigated the influence parameters of flank breakage in bevel gears. He identifies — beyond the known influence of load conditions — case depth and core hardness as important parameters. Analysis of damage patterns of test and practical gears showed that the initiating crack always started below the surface; i.e., in the region of the transition from case to core. For unidirectional loading, the crack propagates to the active flank on one side and to the tooth root on the other. Annast analyzed the subsurface stresses with *ROSLCOR* (*Rolling and SLinding Contact according to OsteR*) (Refs. 9 and 17) by using the shear stress intensity hypothesis according to Tobie (Ref. 18). Oster (Ref. 17) defined, on the basis of (Ref. 21), the potential for considering compressive stresses in the case for the evaluation of the material expo-

Figure 1   Flank breakage and pitting on wheel.

Figure 2   Flank breakage — two different wheels.

sure. Tobie expanded this method with the possibility of including tensile, residual stresses (in the core) as well. However, the overriding influence of tensile-residual stresses simulated by the Tobie model could not be validated in any other investigation (e.g., ANSI/AGMA 2003–B97). Annast argued that it is sufficient to analyze only the section between the flank surface and the transient region of case and core. Indeed, tensile residual stresses were therefore not examined by Annast. In his proposed standard-capable method, only the region-of-transition is regarded. A critical ratio between the acting maximum shear stress and the core hardness was derived from the test gears and practical applications; if the ratio exceeds the limit, the risk of flank breakage is considered high.

Because of the uncertainties in the methods described above, a new calculation method was proposed by Wirth (Ref. 20) for the rating of bevel and hypoid gears. The method is based on Oster's and Hertter's work (Ref. 8). Hertter proposed for cylindrical gears an enhanced shear stress intensity hypothesis to evaluate the subsurface stresses — even under consideration of compressive and tensile residual stresses; a separate examination of dynamic and static exposure allows for consideration of fatigue failures, as well as failures from yielding. Because the local allowable strength values in the considered material element are derived from the hardness by means of material-physical relations, the new method is termed the "material-physical-based calculation method." Wirth adapted Hertter's method to bevel and hypoid gears, considering their specifics as, for example, sliding conditions.

Figure 3   Stress conditions inside the tooth.

Figure 4   Time–dependent stress components in a rolling contact.

Material-Physically Based Calculation Method for Bevel and Hypoid Gears

The material-physical-based calculation method allows the consideration of complex stress conditions beneath the flank surface that are caused by the load and heat treatment process. The permissible stresses are derived from the hardness values and material-physical parameters. The occurring stresses are compared with the permissible stresses in discrete sections in the material. On the basis of a shear stress intensity hypothesis (SIH), the material exposure is determined.

General stress conditions in the tooth. Inside the tooth, beneath an ideal smooth flank surface, the total stress conditions are composed of:
- Stresses due to normal contact load (Hertzian theory)
- Shear stresses on the surface caused by friction
- Thermal stresses caused by the thermal gradient
- Stresses caused by bending mechanism
- Residual stresses

Figure 3 illustrates the stress components that influence the material exposure in a considered (infinitely small) element.
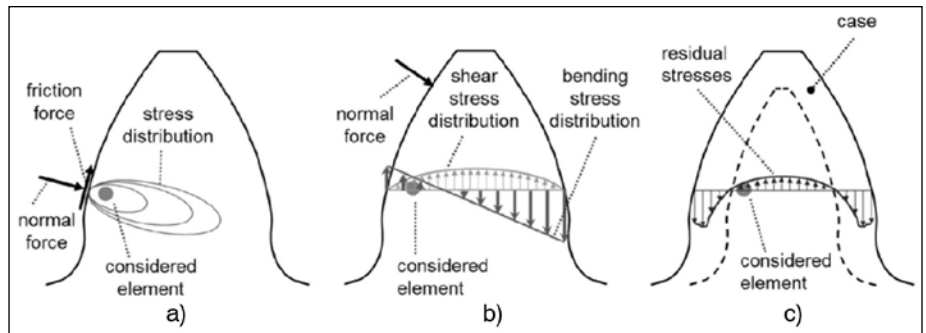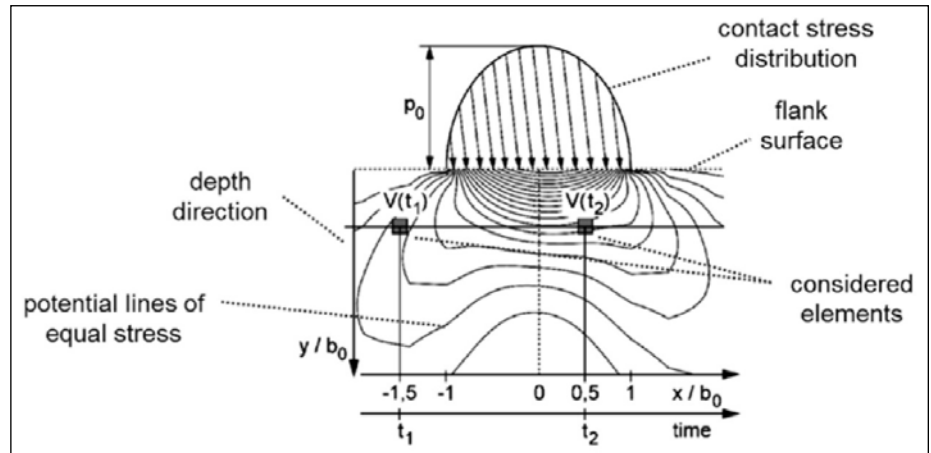
In Figure 3a the stress components that result from the normal load on the flank are shown; the stresses according to Hertzian theory originate at the normal force. Due to the sliding components, the friction force that is tangential to the flank surface induces shear stresses. Figure 3b demonstrates the effect of bending by a normal force that acts above (in profile direction) the considered element. The components of the normal force cause normal stresses, with an approximately linear distribution over the tooth thickness and shear stresses, and with an approximately parabolic distribution and a maximum (distribution) in the middle of the tooth. Residual stresses result from the hardening and finishing process; as an example, Reference 20 shows that compressive stresses are occurring in the case and are balanced by tensile stresses in the core. Unlike the stresses in Figure 3a and Figure 3b, the residual stresses in Figure 3c are load-independent.

Oster and Hertter developed the *STRORHR* program for the calculation of all mentioned stress components on cylindrical gears. With this program it is possible to examine the material exposure in the sub-surface, below any contact point on the flank surface. Thus the examination direction is perpendicular to the flank surface.

Stress Conditions in the Rolling Contact

In any contact point on the flank, the rolling direction *x* can also be seen as the time axis. Figure 4 shows in principle the stress components under the surface. All volume elements in the same depth are exposed to equal stresses — but at different times. To evaluate the material exposure in a certain depth beneath the

flank surface, the corresponding stresses have to be considered over the entire time axis (*x* axis).

However, in rolling contacts a turning principal coordinate system complicates the evaluation of the material utilization. A possible alternative is analyzing the dynamic stresses in rolling contacts; i.e., the shear stress courses in a sectional plane that are defined on the surface of the base sphere (Fig. 5).

Figure 6 shows for a rolling contact an example of shear stress courses in a certain sectional plane γα and a material depth of $y/b_0 = 0.3$; $\tau\gamma\alpha\,(t_i)$ is the time-dependent graph for the projection of shear stresses in the directions n_2 and n_3 (Fig. 5). In Figure 6a no residual stresses are considered; as a consequence the point (0/0) is part of the course. At a certain time t_i — when the contact is still unloaded (e.g., the contact point of the flank surfaces is still far away from the regarded volume element) — $\tau_2 = \tau_3 = 0$ in the examined sectional plane. During the movement of the contact over the flank surface, the stress components τ_2 and τ_3 can be marked in the diagram. Of course if the influence of the moving contact point on the stresses at the examined plane is diminishing, the course will again reach point 0/0. As Figure 6a shows, the instantaneous stress vector (τ_2/τ_3) is completely turning during one load cycle, which means that it acts as an alternating load. Its maximum length is defined as the "maximum shear stress" $\tau_{max,a}$. The diameter of the circumscribed circle is $\Delta\tau_{max,a}$.

Figure 6b shows for the same examined sectional plane an equal load cycle, but in consideration of the residual stresses. Unlike before, the shear stresses τ_2 and τ_3 have discrete val-

ues — even if the contact is unloaded. However, the course of the pair of values τ_2/τ_3 is similar, meaning that $\Delta_{\tau max,a} = \Delta_{\tau max,b}$. An important fact is that the maximum shear stress $\tau_{max,b}$ is decreasing under the influence of (compressive) residual stresses ($\tau_{max,b} < \tau_{max,a}$). In other words, the maximum shear stress with high compressive residual stresses is smaller than the maximum shear stress without residual stresses. This is also valid for other sectional planes of the base sphere and corresponds with the accepted fact that compressive residual stresses reduce the maximum material exposure (e.g., Ref. 22).

The aim of a strength hypothesis is the evaluation of stresses occurring in the examined base sphere (or base element) to determine a number for the material exposure that correlates well with the failure mechanism. Many common criteria are not applicable for alternating stresses, as described before; various important hypotheses are discussed regarding their applicability for the rating of the material exposure in rolling contact. As a result of the investigation, a modified SIH was established (Ref. 8). This hypothesis can principally be used for:
- Rating the maximum exposure of the material (analysis regarding yielding)
- Rating the dynamic exposure of the material (analysis regarding fatigue)

Modified Shear Stress Hypothesis by Hertter (Ref. 8)
The bases for calculation of the decisive exposure in the examined base sphere are the stress courses in all of its sectional planes. According to (Ref. 12), in every sectional plane the normal stresses (orthogonal to sectional plane) can be calculated according to Equations 3 and 4. The shear stresses $\tau\gamma\alpha_a$ and $\tau\gamma\alpha_m$ are defined (Fig. 7) for the considered sectional plane. The radius of the smallest circumcircle of the stress course is the decisive amplitude of the shear stress. (*Ed.'s Note: The circumscribed circle — or circumcircle — of a polygon is a circle which passes through all the vertices of the polygon.*) The vector of its center point represents the mean shear stress.

Amplitude of shear stress (Fig. 7):

$$\tau\gamma\alpha_a = \tau_a(\gamma,\alpha) \tag{1}$$

Amplitude of shear stress (Fig. 7):

$$\tau\gamma\alpha_m = \tau_m(\gamma,\alpha) \tag{2}$$

Amplitude of normal stress: $\sigma\gamma\alpha_a = \sigma_a(\gamma,\alpha)$

$$\sigma_a(\gamma,\alpha) = \frac{\sigma_{max}(\gamma,\alpha) - \sigma_{min}(\gamma,\alpha)}{2} \tag{3}$$

Mean value of normal stress: $\sigma\gamma\alpha_m$ $\sigma_m(\gamma,\alpha)$

$$\sigma_m(\gamma,\alpha) = \frac{\sigma_{max}(\gamma,\alpha) - \sigma_{min}(\gamma,\alpha)}{2} \tag{4}$$

Dynamic exposure in sectional plane: $A(\gamma,\alpha)$

$$A(\gamma,\alpha) = \sqrt[\mu]{\frac{\alpha\,\tau_a^\mu(1 + m\,\tau_m^\mu) + b\,\sigma_a^\mu}{\sigma_A^\mu}} \tag{5}$$
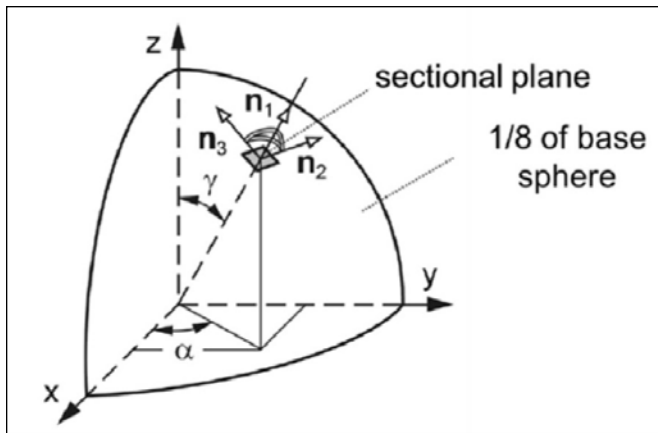
Total dynamic exposure, $A_{int\,a}$

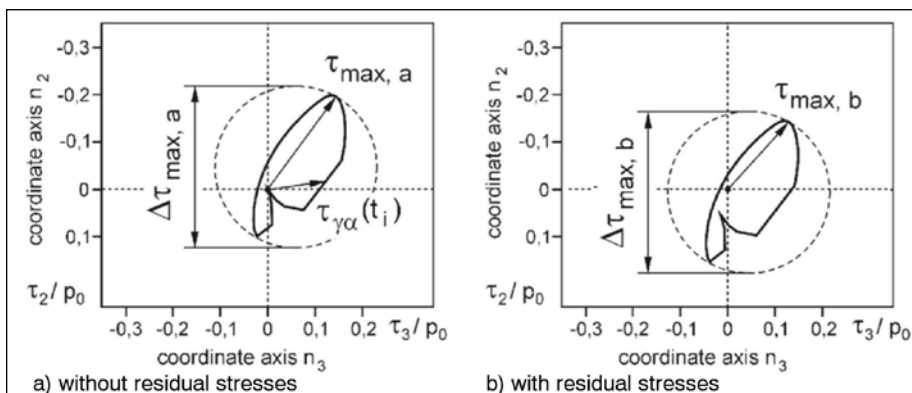**Figure 5   Base sphere with sectional plane (Ref. 8).**

Figure 6   Example of shear stress courses in a sectional plane αγ in the depth y/b$_0$ = 0.3 for rolling conditions (Ref. 8).
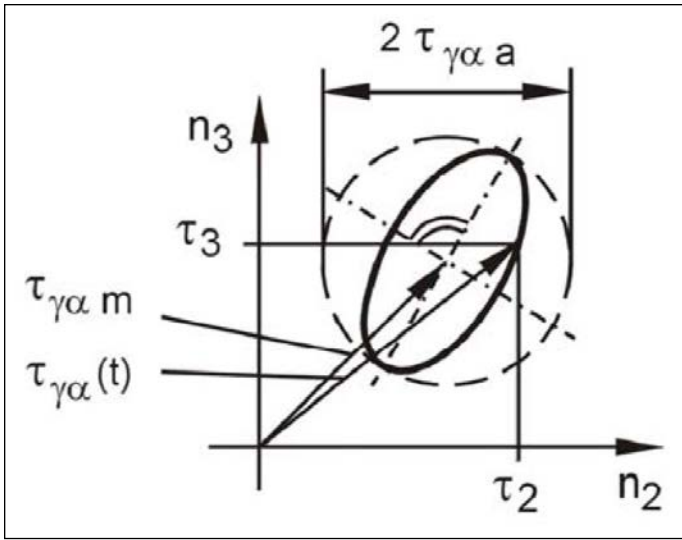
Figure 7 Definition of amplitude and mean value of any shear stress curve plotted over time in a discrete sectional plane (Ref. 8).

$$A_{int\,a} = \sqrt[\mu]{\frac{15}{8\pi} \int_{\gamma=0}^{\pi} \int_{\alpha=0}^{2\pi} \left([A(\gamma,\alpha)]^2 \sin\alpha\right) d\alpha d\gamma} \qquad (6)$$

Maximum exposure in sectional plane, $A_{max}(\gamma,\alpha)$

$$A_{max}(\gamma,\alpha) = \sqrt[\mu]{\frac{\alpha\,\tau_{max}^\mu + b\,\sigma_{max}^\mu}{R_{p0,2}^\mu}} \qquad (7)$$

Total maximum exposure, $A_{int\,a}$

$$A_{int\,a} = \sqrt[\mu]{\frac{15}{8\pi} \int_{\gamma=0}^{\pi} \int_{\alpha=0}^{2\pi} \left([A_{max}(\gamma,\alpha)]^2 \sin\alpha\right) d\alpha d\gamma} \qquad (8)$$

Constant a

$$a = \frac{1}{5}\left[3\left(\frac{\sigma_W}{\tau_W}\right)^2 - 4\right] \qquad (9)$$

Constant b

$$b = \frac{1}{5}\left[6 - 2\left(\frac{\sigma_W}{\tau_W}\right)^2\right] \qquad (10)$$

Constant m

$$m = \frac{1}{\alpha}\left[\frac{\sigma_W^2 - \left(\frac{\sigma_W}{\tau_W}\right)^2\left(\frac{\tau_{Sch}}{2}\right)^2}{\frac{12}{7}\ \left(\frac{\tau_{Sch}}{2}\right)^4}\right] \qquad (11)$$

where:

$\tau_a(\gamma,\alpha)$ is amplitude of shear stress in sectional plane, N/mm^2
  γ is angle for sectional plane (Fig. 5), degrees
  α is angle for sectional plane (Fig. 5), degrees
$\tau_m(\gamma,\alpha)$ is mean value of shear stress in sectional plane, N/mm^2
$\sigma_a(\gamma,\alpha)$ is amplitude of normal stress in sectional plane, N/mm^2
$\sigma_{max}(\gamma,\alpha)$ is maximum of normal stress in sectional plane, N/mm^2
$\sigma_{min}(\gamma,\alpha)$ is minimum of normal stress in sectional plane

$\sigma_m(\gamma,\alpha)$ is mean value of normal stress in sectional plane, N/mm^2
$A(\gamma,\alpha)$ is dynamic exposure in sectional plane
  μ is constant exponent $\mu = 2$
  b is constant (material-dependent)
  σ_A is material amplitude strength according to normal stress, N/mm^2 (Ref. 8)
$A_{int\,a}$ is total dynamic exposure of base sphere
$A_{max}(\gamma,\alpha)$ is maximum exposure in sectional plane
  $R_{p0,2}$ is yield strength, N/mm^2
  A_{int} is total maximum exposure of base sphere
  a is constant (material-dependent)
  σ_W is material alternate strength according to normal stress, N/mm^2 (Ref. 8)
  τ_W is material alternate strength according to shear stress, N/mm^2 (Ref. 8)
  m is constant (material-dependent)
  τ_{Sch} is material pulsating fatigue strength, N/mm^2 (Ref. 8)

With the stress values according to Equations 1–4, the material exposure $A(\gamma, \alpha)$ in the considered sectional plane can be calculated (Ref. 8). The local amplitude strength σ_A is dependent on the mean value of normal stress $\sigma_m(\gamma, \alpha)$. The constants a, b and m are a function of the strength ratio σ_W/τ_W and the local torsional pulsating fatigue strength τ_{Sch} (Ref. 12).

The total dynamic exposure $A_{int\,a}$ is defined as the integral value of the exposure values $A(\gamma, \alpha)$ in all sectional planes and determined by Equation 6. The endurance limit of the considered element regarding fatigue is, per definition, reached when the total dynamic exposure becomes $A_{int\,a} = 1$. Values below stand for infinite life. In an analogous way, the maximum exposure regarding yielding is calculated (Eq. 7). For all sectional planes in the base sphere, the total maximum exposure for yielding is considered according to Equation 8. Again, for an infinite life the total maximum exposure has to fall below $A_{int} < 1$.

It is remarkable that all local strength values can be determined out of the Vickers hardness values by means of material-physical-based relations (Ref. 8).

Calculation Process for Bevel and Hypoid Gears: Overview

As described above, Hertter (Ref. 8) developed for cylindrical gears the material-physical-based method to evaluate the material exposure in the sub-surface of the tooth. The strength values are, accordingly, derived from the Vickers hardness test relative to volume element (base sphere).

The comparison of the local stress values with the local strength values provides a 3-D evaluation of the material exposure — not only close to the flank surface but also in an area close to the core. Whereas the allowable stress numbers according to ISO, DIN or AGMA are only valid for an optimally designed case depth, the material-physical-based method allows investigation of the influence of different hardness profiles on load capacity. Moreover, due to the local consideration of the material exposure, the failure mode becomes apparent.

Hertter expanded the computer program *ROSLCOR* (*Rolling and SLiding Contact according to OsteR* (Refs. 9 and 17)) that was developed at the FZG (Gear Research Center of the Technical University of Munich) with his material-physical-

based method; Wirth (Ref. 20) adapted Hertter's method to bevel and hypoid gears. Wirth developed the computer tool *LokAna* (*Local Analysis*) that handles not only the sub-programs *BECAL (Bevel Gear Calculation)* (Ref. 10) and *ROSLCOR,* but also further calculations for bevel gears.

Calculation of Material Exposure

The Hertzian stresses on the flank surface of bevel and hypoid gears are determined with the FVA program *BECAL* (*Bevel Gear Calculation*) (Ref. 10). With the machine settings for the gear set, *BECAL* is able to generate the geometry of flank surface and tooth root. Based on this information a loaded tooth contact analysis (TCA) leads to the tooth root stresses and to the local-occurring Hertzian stresses; deflections of housing, bearings and shafts can be also considered.

For any calculated point on the flank — the partial line of contact, its relative curvature, the acting normal force, and Hertzian stress — are determined. For *ROSLCOR*, the considered contact point can be simplified to a contact of an infinite long cylinder with a half-plane (Fig. 8).

In the stress calculation with *ROSLCORHR* (Ref. 8) — an enhancement of *ROSLCOR* — the normal stresses and shear stresses resulting from bending (Fig. 3b) are addressed. The acting normal force that moves over the flank surface causes — at any later stage — normal stresses and shear stresses in the considered volume element (base sphere). For the material exposure, the maximum values over one load cycle have to be considered.

The stresses caused by the normal load in the sub-surface are calculated with the model shown (Fig. 8 — right). The basis for the stress mechanics is the plain strain state, meaning that deformations are only allowed in a plane vertical to the contact line. *ROSLCOR* considers the normal pressure on the surface as well as the influence of a loss-of-friction contact. The influences of thermal stresses and shear stresses on the material exposure are also addressed.

The material-physical-based calculation model evaluates for a certain volume element the risk for an initial crack. Whether the crack will result in damage of the flank or not is dependent on its potential for crack growth; especially near the flank surface, this potential is affected by the slip conditions in the contact point. As is known (Refs. 14 and 19), pitting occurs mainly in the flank area with negative slip, which is below the pitch point for pinion and wheel at bevel gears without offset. Deeper below

the flank surface the influence of slip in the contact point seems, as is known thus far, negligible.

Wirth (Ref. 20) introduced a so-called "slip factor" that accounts for the difference in strength between negative and positive slip conditions. The influence of this factor is restricted to the material close to the surface. Because the material strength values are derived from the material hardness, it is allowable to (virtually) increase the hardness values appropriately. Consequently, for the same load conditions the material exposure in flank areas with positive slip is lower than in areas with negative slip. The hardness values are modified by Equations 12–14. Wirth demonstrated that reasonable results are calculated if $a/b_0 = 0.5$ and $b/b_0 = 1.0$ are chosen (b_0: half of the Hertzian contact width, Fig. 8).

Depth range $0 < y < a$:

$$HV(y) = HV_0(y)\, Z_{S1,2} \tag{12}$$

Depth range $y > b$:

$$HV(y) = HV_0(y) \tag{13}$$

Depth range $a \leq y \leq b$.

$$\text{Linear interpolation of } Z_S \tag{14}$$

where:

y is material depth below the contact point, mm

a is certain material depth, mm

$HV_{(y)}$ is modified local hardness in consideration of the slip influence, HV

$HV_0(y)$ is local hardness, HV

b is certain material depth, mm

Z_S is factor according to (Ref. 20)

Residual stresses in the tooth. Hertter demonstrated that the influence of residual stresses has to be considered in the material exposure (Fig. 6) for the evaluation of tooth failures. In particular, the maximum material exposure A_{int} is influenced by the residual stresses. Whereas compressive stresses typically have a positive effect on the material exposure, tensile stresses increase the material stresses (Ref. 8). The total dynamic exposure $A_{int\,a}$ is only influenced by means of the mean stress sensitivity. As Hertter proved, the material exposure in the range of the transition zone from case to core accounts for failure modes like flank breakage that are usually characterized by an initial crack in this region.

Wirth (Ref. 20) proposes adoption of the (compressive) residual stresses according to Lang (Ref. 11) for the case. Due to the balance of forces in the core, tensile residual stresses have to exist. For the estimation of the residual stress distribution in the core, Wirth made investigations based upon finite element (FE) methods. Using a parabola of the fourth degree, the tensile stresses can be closely approximated by the balance of forces. Figure 9 shows qualitatively in a normal section of the tooth the residual stress distribution. It is a sufficient correlation that the residual stresses in tooth height direction are equal to the residual
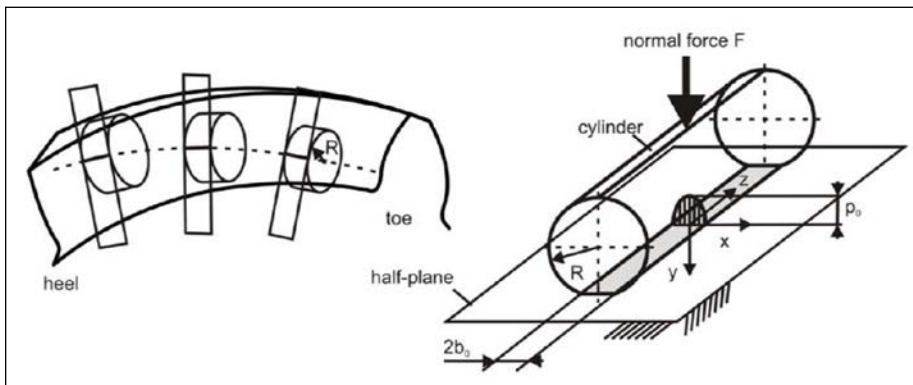

Figure 8   Simplification of complex contact conditions — cylinder model.

stresses in lengthwise direction. Residual stresses in the orthogonal direction to the flank surface may be ignored.

Improvement of a Gear Set with Flank Breakage

Wheel flank breakage. A decisive number of hypoid gear sets used in axle gear drives in test vehicles failed due to flank breakage; only the wheels were affected by this failure mode. Figure 1 (left side) shows a flank breakage on one tooth of a wheel; in Figure 1 (right side) pitting on the coast-side could be detected. Figure 2 shows on another wheel a characteristic flank breakage; as can be seen, the failure plane runs on both flank sides through the active tooth height.

To learn more about the conditions where and when flank breakages occur, a new type of test for the stationary test rig has been developed and comprehensive test runs conducted. The gear sets have been tested for a defined load spectrum where the highest load stage was the torque that has been considered in the following calculations. The gear sets failed—either by pitting or flank breakage. Pitting occurred on the pinion as well as on the wheel; flank breakage was only observed on the wheel.

Figure 10 shows for a damaged wheel the investigation of the fracture surface in the scanning electron micrograph (SEM). In this case a small inclusion was detected from where the crack propagates to the flank surfaces. Inclusions can be regarded as a catalyst for the crack initiation because of the notching effect of different elasticity moduli. Investigations by Annast (Ref. 1) showed that an Al_2O_3 inclusion causes a stress increase (von Mises criterion) of approximately 30%–40%; the size and the depth beyond the surface have a relatively small influence. Therefore, the lower the material exposure in the core, the smaller the risk of flank breakage with initial cracks in this region will be (Fig. 10).

Design of an improved gear set. The aim of the re-design was to develop a new gear design with a smaller material exposure to avoid flank breakage on one hand and pitting as far as possible on the other. In a first step the old design was analyzed with the newly introduced material-physical calculation method. In the second step a new gear design with same ratio and diameters but lower material exposure was searched by an iterative process. Table 1 contains the main geometry data of the old and new gear design.

For the calculation, discrete contact points on the flank are chosen for the evaluation. Figure 11 shows that the selected contact points are positioned in a section with considerably high load and the suspected crack origin. To evaluate not only the risk of an initial crack at one single point, but also the potential of crack growth, four different positions were examined.
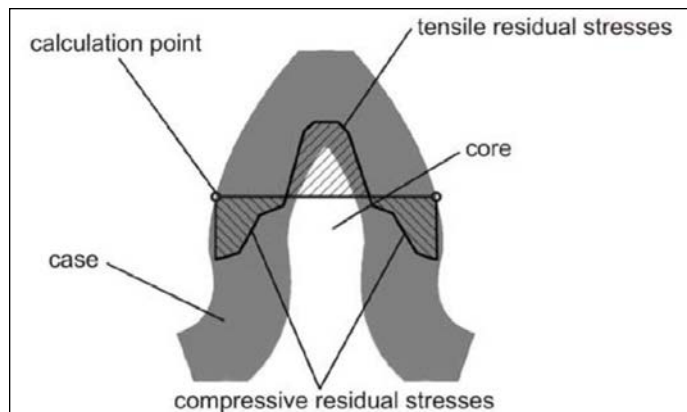

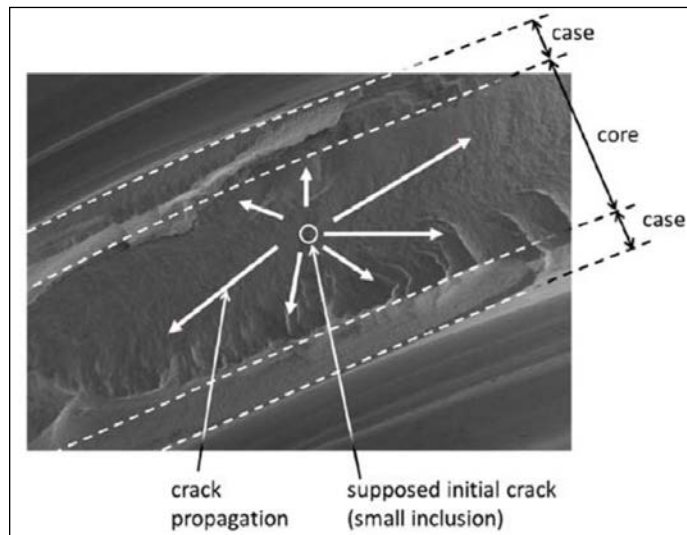Figure 9   Residual stress distribution in the tooth.

Figure 10   Flank breakage—two different wheels.

For Related Articles Search

breakage

at **www.geartechnology.com**

Table 1 Geometry of the examined gear sets			Old design		New design	
Nomenclature	**Symbol**	**Unit**	**Pinion**	**Wheel**	**Pinion**	**Wheel**
Number of teeth	z		8	45	8	45
Pinion offset	a	mm	34		34	
Normal module	m_{mn}	mm	6.134		6.122	
Mean pitch diameter	d_m	mm	69.6	331.2	69.9	332.3
Face width	b	mm	60.7	58.3	62.2	59.0
Spiral angle	β	°	45.5	34	45.5	34
Material			25MoCr4E		25MoCr4E	
Roughness Rz flank/tooth root	Rz	mm	3/16 (after run in)			
Total overlap ratio (under load) drive/coast			3.0/2.7		2.92/2.7	
Lubricant			Shell Spirax ASX 75W 90			
Temperature of lubricant	θ	°C	90			

NOTE: Because only the wheel was affected by flank breakage, all calculations have been made for the wheel only!

Table 2 contains the Hertzian stresses that were determined by means of the loaded tooth contact analysis with *BECAL* (Ref. 10). Deformation and deflections of housing, shafts and bearings have been considered. Under the same load conditions it was possible to reduce the stresses on both flank sides in the critical area of the flank by approximately 15%. This was possible with an optimized crowning ("ease-off") in combination with a different gear design (duplex instead of semi-completing) and changed pressure angles.

Of course the reduction of contact stresses leads in most cases to an increase in load capacity — especially when the failure mode pitting is addressed. But in the case of flank breakage the failure mechanism is influenced by not only the contact stresses, but also by the material exposure deep inside the tooth. Because of the requirement to keep the amount of transferred torque

Figure 11   Contact pattern and calculated contact points on the wheel flanks.

Table 2	Hertzian stress under the considered load calculation			
Calculation point	**Old design**		**New design**	
	Drive side	**Coast side**	**Drive side**	**Coast side**
P1	1,865	1,951	1,629 (-13%)	1,692 (-13%)
P2	1,891	1,979	1,571 (-17%)	1,698 (-14%)
P3	1,841	1,961	1,593 (-13%)	1,651 (-16%)
P4	1,612	1,901	1,553 (-4%)	1,585 (-17%)

Figure 12   Profiles for hardness and residual stress.

by retaining the gear dimensions (and module), the total flank load cannot be significantly reduced. To avoid flank breakage, the goal must be to reduce material exposure — mainly in the core — where, in this case, the crack initiation could be detected in several cases (Fig. 10).

As mentioned earlier in the evaluation of the material exposure in the sub-surface section, especially in the middle of the tooth thickness, the following stress components must not be ignored:
- Shear stresses due to shearing forces (flank normal forces)
- Tensile residual stresses

The shear stress distribution reaches its maximum in the middle of the tooth thickness (Fig. 3b). Also, the maximum values of the tensile residual stresses are supposed to be in this region. Whereas the determination of the shear stresses is strictly a mechanical problem, the residual stresses are caused mainly by the heat treatment process. Only in the area directly beneath the surface are residual stresses influenced by the finishing process of the gear. As such, the residual stresses are derived by the hardness profile described earlier.

Figure 12 shows that, for the following calculations results, the assumed hardness profiles are based on detailed measurements, yet smoothed for calculation. Because of the slightly different cooling conditions during the hardening process in profile direction of the tooth, the hardness gradients and core hardness are slightly different. The derived residual stress distributions are shown as well (Fig. 12). It can be seen that the compressive stresses in the case are up to $\sigma_{res} \approx 400\,\text{N/mm}^2$ and are decreasing up to the transient region of case and core. Because the case thickness in profile direction is more or less constant, the compressive residual stress profiles are similar. In contrast to that, the tensile residual stresses in the middle of the tooth thickness are increasing from P4 to P1. The reason is the mechanical balance of forces; i.e., the separating forces that are caused by the compressive stresses in the case are approximately constant for P1 through P4. The attracting force is represented by the tensile compressive stresses and requires having an equal amount. Because the core section becomes smaller — P4 through P1 — the corresponding tensile stresses must increase.

Figure 13 reveals the calculated material exposure for P1 through P4; the black lines represent the total dynamic exposure A_{inta}; the grey lines represent the total maximum exposure A_{int}.

A_{inta} can be seen as a value to describe the material fatigue; it is based on an endurance strength (derived from the Vickers hardness) for a failure probability of 50%. Pitting is a typical fatigue failure that correlates with the total dynamic exposure A_{inta}. (Ref. 8); (Refs. 18
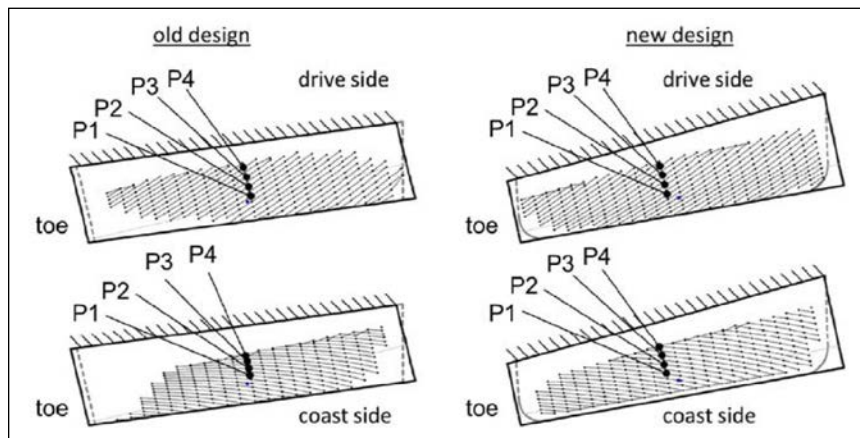
and 20) show that if material exposure values exceed a certain limit in the subsurface — up to a depth of $y/b_0 \approx 1$ (b_0: half of Hertzian contact width) — pitting failure occurs with a high probability. For the examined gear this decisive range is up to approximately $y \approx 1$ mm. As Figure 13 shows, $A_{int\,a}$ exceeds the limit of 1. Due to the load spectrum of the test vehicles, which had only a few time slices with this considered load, pitting failures on the drive-side where not detected. The fatigue strength may be the reason for that.

A_{int} represents the material exposure concerning yielding. According to the theory of the calculation method — $A_{int} > 1$ — local redistribution of stress or initial cracks occurs. This situation is exacerbated if the notching effect of inclusions or incongruities increases the material exposure. At this time there is no possibility provided by the material-physical-based method to address this fact in the calculation process. Therefore the practical limit for A_{int} values that are determined for a homogenous material should be reduced to values smaller than 1 in order to be on the safe side. Because of the specifics of the hardening process, incongruities occur more typically in the core than in the case; this is why the total maximum exposure A_{int} should be limited — especially in the core.

Hertter (Ref. 8) and Wirth (Ref. 20) found good correlation between the total maximum material exposure A_{int} and the failure mode flank breakage. Especially high values in the material depth between the transition of case and core — as well as in the core — seem to cause flank breakage. It must be pointed out that crack initiations caused by yielding have no endurance limit or fatigue strength for finite life. According to theory, only a very few single-load cycles are enough for stress redistribution or crack initiation. These cracks may also have the ability to grow at lower loads. Unlike for the calculation against fatigue where there is a high strength for finite life, it is already critical if an initial crack occurs during a momentary high load. In other words, it is more important to reduce high A_{int}- values (concerning yielding) than the $A_{int\,a}$ values (concerning fatigue) if the gear set is stressed by a load spectrum with only momentary high loads.

Figure 13 shows that A_{int} of P1 exceeds the limit 1 in the depth between $y = 2.5$–3.7 mm. P2 causes values $A_{int} > 0.9$ in a range between $y = 2.2$–4 mm and P3 for $y = 1.5$–3.2 mm. Only the A_{int} graph for P4 is constantly under 0.9. These high values of A_{int} over a very large section of the tooth correlate well with the witnessed flank breakages.

The first evidence of flank breakage does not necessarily appear in a single volume element. Local peaks of material exposure may be reduced after a yielding process and no growing crack is initiated, meaning that the failure mode of flank
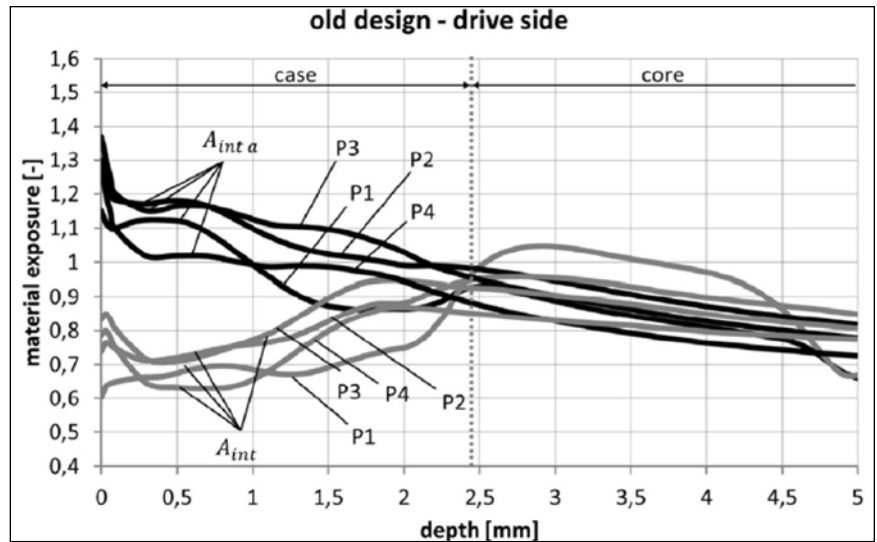

Figure 13   Material exposure for calculated points: old design — drive-side of wheel.
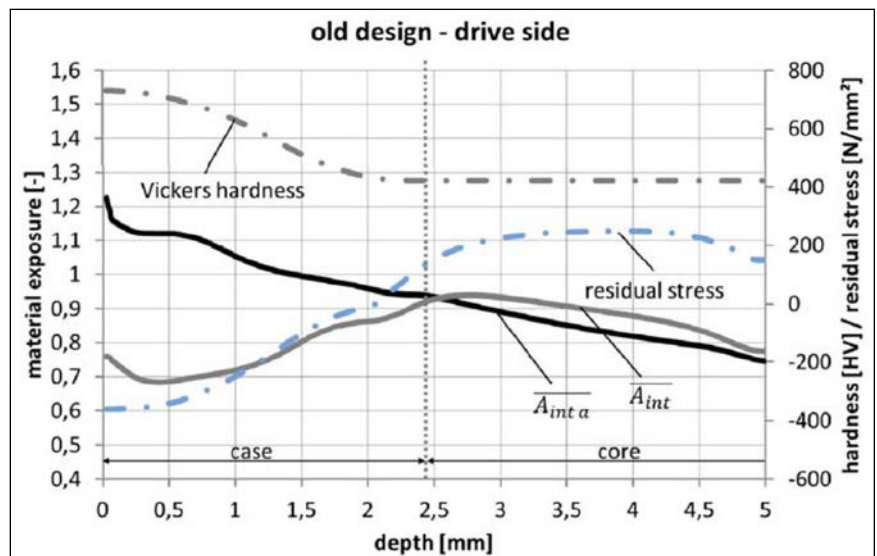

Figure 14   Mean values of material exposure (crack growth potential): old design — drive-side of wheel.

breakage will not occur. Therefore it is not only decisive for flank breakage if in one contact point the limit for yielding is reached; in fact, high values of A_{int} in adjacent contact points support crack growth. In order to evaluate this potential a mean value of the total maximum exposure is defined (Eq. 15). For the four considered contact points the average value of each A_{int} graph is determined in a certain depth. Of course, based on this consideration, determination of the $A_{int\,a}$ mean value is also useful in determining an idea of the pitting danger over the considered flank area.

(15)

$$\overline{A}(y) = \frac{1}{i}\sum_{1}^{i} A_i(y)$$

where:

$\overline{A}$ is mean value of total dynamic exposure $A_{int\,a}$ or mean value of the total maximum exposure A_{int}

y is material depth, mm

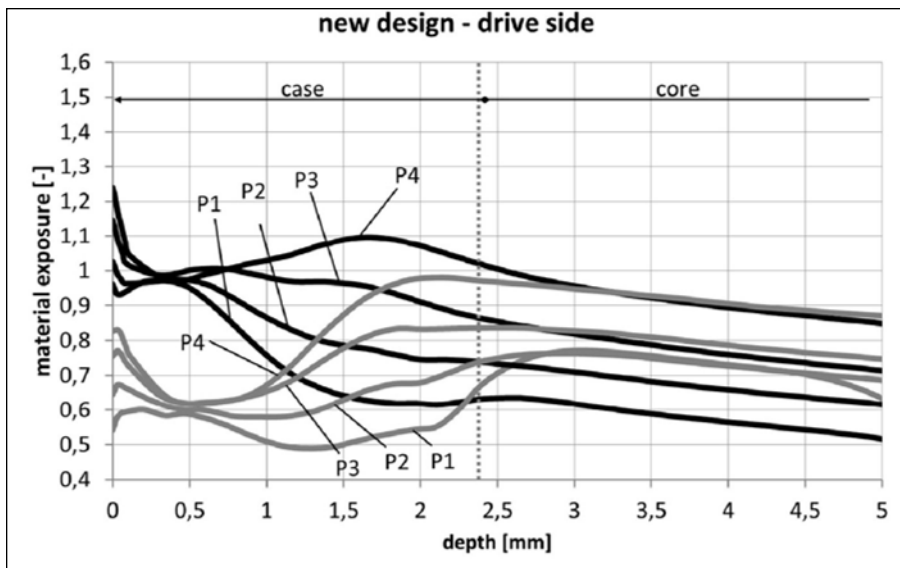i is amount of considered calculation points

Figure 15   Material exposure for calculated contact points: new design — drive-side of wheel.
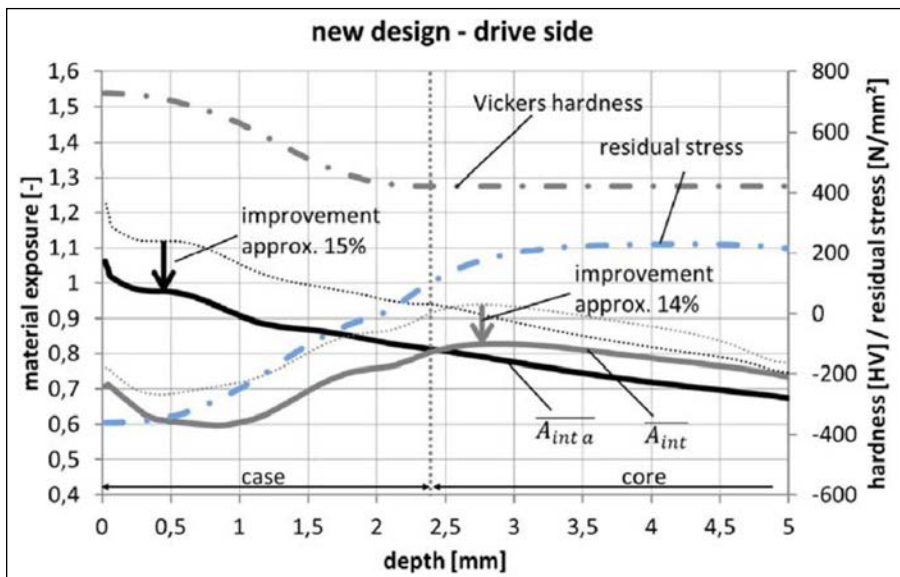

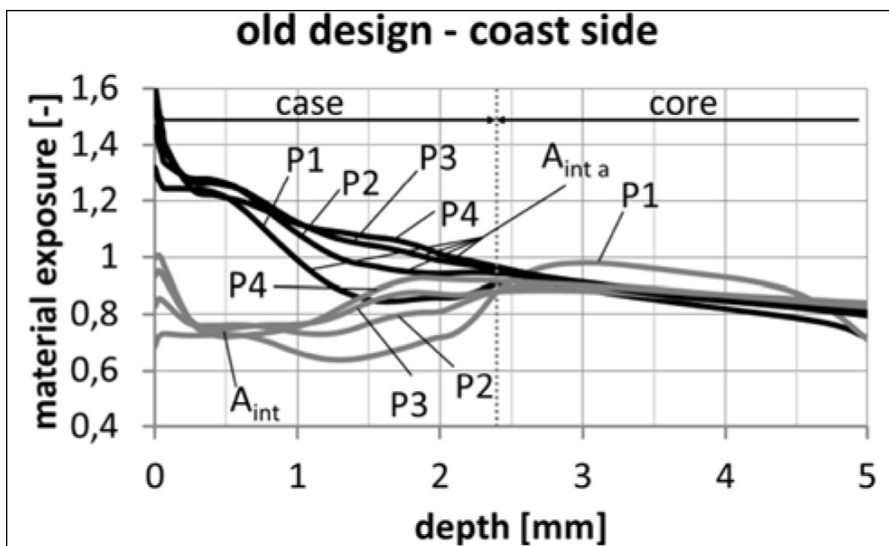**Figure 16   Mean values of material exposure (crack growth potential): new design — drive-side of wheel.**

Figure 17   Material exposure for calculated contact points: old design — coast-side of wheel.

A is total dynamic exposure $A_{int\,a}$ or total maximum exposure A_{int}.

In Figure 14 the graphs of the mean values $A_{int\,a}$ and A_{int} are shown for the drive-side of the wheel flank. It is obvious that in the depth $y < 1\,mm$, $A_{int\,a}$ has considerably high values. As mentioned, this is an explanation for the observed pitting in the field. But more important for flank breakage is, as described before, the profile of A_{int}. It can be seen (Fig. 14) that in the depth $y = 2.3$–$3.7\,mm$, the exposure is $A_{int} \geq 0.9$. Together with the mentioned influence of inclusions like those detected (Fig. 10), it is obvious that there is a high risk of flank breakage under these load conditions. The profiles for hardness and residual stress shown (Fig. 14) are also principally derived by Equation 15 and so can be interpreted as the mean values.

Figure 15 shows for the new design the corresponding calculations for points P1–P4. Compared to Figure 13 it is obvious that in the close region to the surface ($y < 1\,mm$) the total dynamic exposure $A_{int\,a}$ can be reduced. But more critical to the failure mode flank breakage is the reduction of the total maximum exposure A_{int} in the sub-surface of the tooth; the exposure profiles of all considered points do not exceed the theoretical limit of 1. Further, the maxima of A_{int} for the points P1 and P2 are significantly lower.

In Figure 16 the mean values according to Equation 15 are shown for the drive-side of the new design; as mentioned, their values represent the potential for crack growth. It can be seen that in the relevant depth for pitting ($y < 1.0\,mm$), there is a significant reduction of the total dynamic exposure $A_{int\,a}$. For better illustration, the profile of the old design is shown by a dotted line; improvement for pitting can be estimated at approximately 15%. Again, the mean values show also the reduced crack growth potential in the inner tooth. In the transition from case to core the values for the total maximum exposure A_{int} are lowered by approximately 14%.

Finally, it can be said that, for the drive-side flanks of the new design, the exposure profiles $A_{int\,a}$ and A_{int} representing the risk of crack initiation are significantly lower, as are the mean values $A_{int\,a}$ and A_{int} that can be regarded as the potential for crack growth.

Indeed, it is not sufficient to optimize only the drive-side flanks. The specific

load spectra in the practical field show that the coast-side flanks are considerably high-loaded; thus the coast-side is analyzed using the same load as the drive-side.

Figures 17 and 18 show a comparison of the exposure profiles for the old and new gear designs' coast-side flanks. As on the drive-side, the values of $A_{int\,a}$ in the decisive depth for pitting could be significantly reduced. But also in the decisive depth for flank breakage, where the initial crack is suspected (Fig. 10), the maximum exposure A_{int} could be lowered in every considered calculation point.

The old-design, mean values of the exposure profiles are shown (Fig. 19). As can be seen, the $A_{int\,a}$ level regarding pitting ($y < 1.0$mm) is even higher than for the drive-side. This correlates well with the pitting that was observed on several gears of the test vehicles (Fig. 1). Regarding the crack growth potential for flank breakage, the mean values for the exposure A_{int} are similar to those on the drive-side. This means that initial cracks close to the middle of the tooth thickness can grow for drive-side as well as for coast-side loading.

Figure 18 proves that the decisive $A_{int\,a}$ values for pitting could be clearly decreased, and is confirmed by the mean values $A_{int\,a}$ (Fig. 20). Further, the risk of crack initiation in the subsurface $y > 1.5$mm is lowered for every considered point (Fig. 18); this obviously leads to an improved situation for crack growth potential. As shown (Fig. 20), the mean values A_{int} could be reduced by approximately 11% with the new design.

Because of the positive prediction in load capacity—especially concerning flank breakage and pitting—prototype gear sets based on this new design have been produced and analyzed in the test rig. The gears were loaded by the same load spectrum. The main goal—avoiding flank breakage—was attained. What's more, pitting on wheel flanks did not occur during the tests. Though the pinion is now failing via pitting, the run time could be stretched by approximately a factor of four.

Summary

- Flank breakage occurred on the wheel of several bevel gear sets used in test vehicles of MTB. In some cases the damage was accompanied by pitting on several wheel flanks. Tests on a MTB test rig confirm that this type of failure is reproducible for a certain load spectrum.
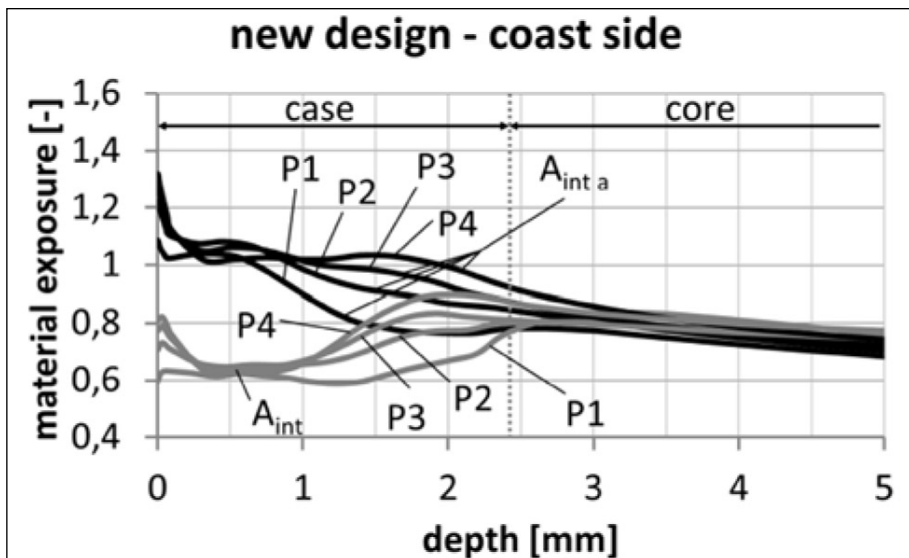
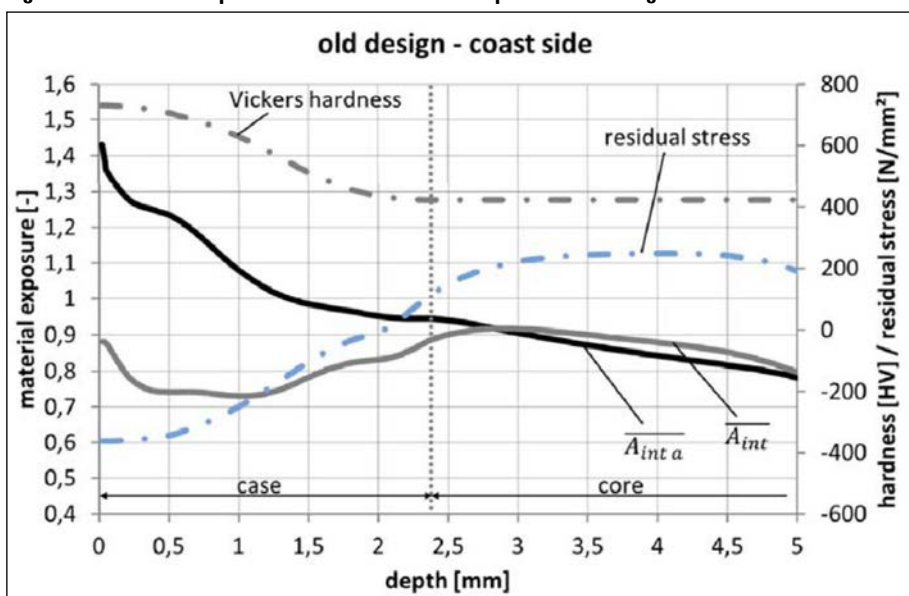Figure 18   Material exposure for calculated contact points: new design—coast-side of wheel.

Figure 19   Mean values of material exposure (crack growth potential): old design—coast-side of wheel.

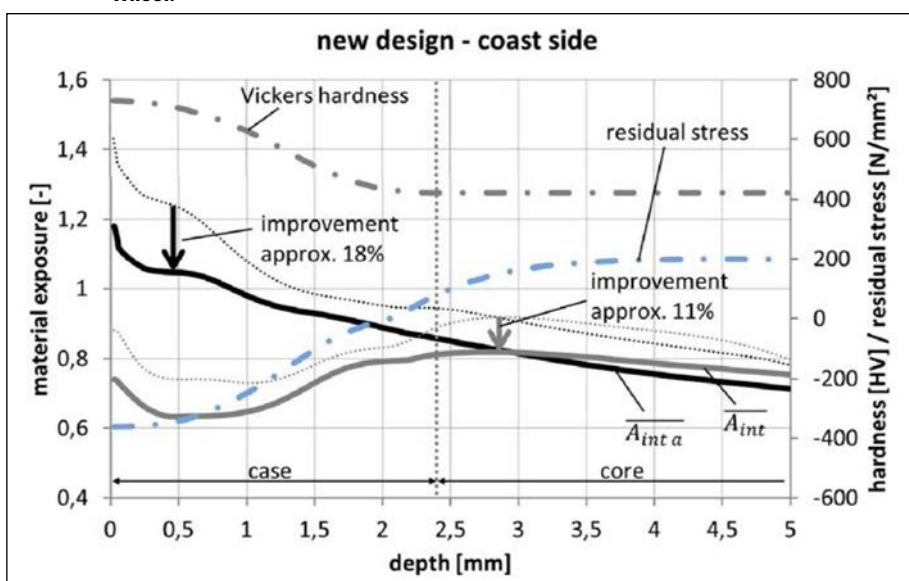

Figure 20   Mean values of material exposure (crack growth potential): new design—coast-side of wheel.

- The goal of a new gear design was to avoid flank breakage in all circumstances and to increase pitting-related load capacity. Because it was essential to retain the outer wheel diameter, the pinion offset and gear ratio — mostly the micro-geometry of the corresponding flanks (ease-off) — were modified. To reduce the amount of test gears needed during the re-design process, a new calculation model was used to evaluate the risk for flank breakage and pitting on the basis of a loaded TCA.
- The new calculation model was introduced by Hertter (Ref. 8) for cylindrical gears — and expanded by Wirth (Ref. 20) — taking into account the specifics of bevel and hypoid gears. The new method is based on material-physical relationships and allows for the evaluation of material exposure in the sub-surface. The influences of local hardness (via hardness profile) and residual stresses can be explored. As demonstrated — (Refs. 18, 8 and 20) — the material exposure in the depth closest to the surface is decisive for pitting failure. On the other hand, extensive material exposure in the transient region from case to core, or in the middle of the tooth thickness, seems to affect flank breakage.
- With this new model, the risk of pitting and flank breakage failures can be better predicted. But while pitting resistance can be predicted with good accuracy, a consistently successful calculation of the load capacity regarding flank breakage is virtually impossible. Uncertainties in the calculation model include the influences of inclusions and/or material discontinuities on the material exposure. Furthermore, the tensile residual stresses that have a decisive influence are estimated by reliance on a simple model. However, FE analysis could improve the prediction quality of the model. Ultimately, the comparison of the load capacity of two gear designs produced in a similar way is reliably doable.
- In an iterative process, new gear designs have been analyzed with the material physical calculation method. The result is a new gear set with significantly lower risk of failing due to pitting or flank breakage; testing with first-prototype gear sets confirmed the improvement. Neither pitting nor flank breakage occurred during the previous test runs. ⚙

References

1. Annast, R. "Kegelrad — Flankenbruch," Diss., TU München.
2. ANSI/AGMA 2003–B97. Rating the Pitting Resistance and Bending Strength of Generated Straight-Bevel, Zerol-Bevel and Spiral-Bevel Gear Teeth.
3. Batista, A.C., A.M. Dias, J.L. Lebrun, J.C. Le Flour and G. Inglebert. "Contact Fatigue of Automotive Gears: Evolution and Effects of Residual Stresses Introduced by Surface Treatments," *Fatigue Fract. Engng. Mater. Struct.* 23 (2000), S. 217–228.
4. Coleman, W. "Bevel and Hypoid Gear Surface Durability, Pitting and Scuffing," *Proceedings, Institution of Mechanical Engineers*, Paper 13, 1967–69, Volume 182, Part 3A, Gleason Works, Rochester, NY.
5. Dudley, D.W. and H. Winter. "Zahnräder-Berechnung, Entwurf und Herstellung nach Amerikanischen Erfahrungen," Springer Verlag, Berlin, 1961.
6. Elkholy, A. "Case Depth Requirements in Carburized Gears," *Wear,* 88, 1983, S. 233–244.
7. Gärtner, J. "Betriebsverhalten Hochbelasteter Kegelradsätze in Traktoren," *Berichtsband zur Tagung Innovationen Rund ums Kegelrad,* Aachen, 10.–11.3.1998.
8. Hertter, T. "Rechnerischer Festigkeitsnachweis der Ermüdungstragfähigkeit Vergüteter und Einsatzgehärteter Stirnräder," Diss., TU München, 2003.
9. Höhn, B.–R. and P. Oster. "Der Flankenkontakt ein Elastohydrodynamischer Wälzkontakt," VDI–Berichte 1207, 1995, S. 93–106.
10. Hutschenreiter, B. "Ergänzung der Berechnungsmöglichkeit von *BECAL* für Flankenmit Negativem Höhenballigkeitsradius und Kopfrücknahme," Abschlussbericht und Handbuchergänzung D zur Version 3.4.0., FVA—Forschungsheft, No. 548, Forschungsvereinigung Antriebstechnik e.V., 2007.
11. Lang, O.R. "Berechnung und Auslegung Induktiv Randschichtgehärteter Bauteile," In, Kloos, K.H. (Hrsg.), Grosch, J. (Hrsg.), Induktives Randschichthärten, Tagung 23., bis 25., März 1988, München, AWT, 1989, S. 332–348.
12. Liu, J. "Beitrag zur Verbesserung der Dauerfestigkeitsberechnung bei Mehrachsiger Beanspruchung," Dissertation, TU Clausthal, 1991.
13. Pederson, R. and R.L. Rice. "Case Crushing of Carburized and Hardened Gears," *Trans. SAE*, 1961, S. 360–370.
14. Rösch, H. "Untersuchungen zurWälzfestigkeit von Rollen: Einfluss vonWerkstoff,Wärmebehandlung und Schlupf," Diss., TU München, 1976.
15. Sandberg, E. "A Calculation Method for Sub-Surface Fatigue," *International Symposium on Gearing and Power Transmissions*, Tokyo, 1981, Volume 1, S. 429–434.
16. Sharma, V.K., D.H. Breen and G.H. Walter. "An Analytical Approach for Establishing Case Depth Requirements in Carburized and Hardened Gears," *Transaction of ASME for presentation at the Design Engineering Technical Conference*, Chicago, Illinois, September 26–30, 1977.
17. Oster, P. "Beanspruchungen der Zahnflanken unter Bedingungen der Elastohydrodynamik," Dissertation,TU München, 1982.
18. Tobie, T. "Zur Grübchen: und Zahnfußtragfähigkeit Einsatzgehärteter Zahnräder," Dissertation, TU München, 2001. Wirth, C. "Entwicklung eines Berechnungsverfahrens zur Grübchen: und Zahnfußtragfähigkeit von Hypoidrädern," Forschungsvereinigung Antriebstechnik e.V., Heft 887, Frankfurt, 2009.
19. Wirth, C. "Zur Tragfähigkeit von Kegelrad: und Hypoidgetrieben," Diss., TU München, 2008.
20. Zenner, H. and I. Richter. "Eine Festigkeitshypothese für die Dauerfestigkeit bei beliebigen Beanspruchungskombinationen," *Konstruktion* 29, 1977, S. 11–18.
21. Zwirlein, O. and H. Schlicht. "Werkstoffanstrengung bei Wälzbeanspruchung— Einfluss von Reibung und Eigenspannungen," Z. Werkstofftech. 11, 1980, S. 1–14.

Dr. Christian Wirth has since 2011 served as managing director of Zahnräder und Getriebe GmbH. Previously, beginning in 2008, he was research group leader at the Gear Research Laboratory of the Technical University of Munich (FZG) before being named technical manager at Zahnräder und Getriebe. From 2002 until 2008 Wirth was a scientific assistant at Technical University of Munich (FZG), where he received his mechanical engineering and PhD degrees (thesis: the load capacity of bevel and hypoid gears).

Bernd-Robert Höhn studied mechanical engineering at the Technical University Darmstadt (1965-1970) and served as an assistant lecturer (1970-1973) at the Institute for Machine Elements and Gears at the Technical University Darmstadt prior to becoming an assistant professor at the university (1973-1979); in 1978, he received his PhD (Dr. Ing.) in mechanical engineering. In early April, 1979 Höhn worked as a technical designer in the department for gear development of the Audi, and by 1982 was head of the department for gear research and design for the automaker. In 1986 Audi named Höhn department head for both gear research and testing of automotive transmissions, until his departure in 1989 to become head of both the Institute of Machine Elements at the Technical University and of the Gear Research Centre (FZG). Höhn has served since 2004 as vice president for VDI for research and development and since 1996 has led the working group 6 and 15 for ISO TC 60—calculation of gears.

Dr. Christo Braykoff received his degree in mechanical engineering from the Technical University of Sofia and the Technical University of Karlsruhe in 2001. From 2001–2007, he worked at the Gear Research Centre (FZG) and obtained his PhD on the topic, Load-Carrying Capacity of Fine-Module Gears. He has worked since 2007 at MAN Truck & Bus AG as a design engineer and is responsible for the development of driven rear axles and transfer cases of trucks and buses. Dr. Braykoff is an active member of the FVA working groups "Bevel Gears" and "Spur Gears" and has since 2008 been a member of the FVA scientific advisory board as MAN representative.